Published in "ChemSusChem 12(21): 4846–4853, 2019"
which should be cited to refer to this work.

New $Ni_{0.5}Ti_2(PO_4)_3$@C NASICON-type Electrode Material with High Rate Capability Performance for Lithium-Ion Batteries: Synthesis and Electrochemical Properties

Mohammed Srout,[a, b] Nam Hee Kwon,[b] Wen Luo,[d, e] Andreas Züttel,[d, e] Katharina M. Fromm,[b] and Ismael Saadoune*[a, c]

$Ni_{0.5}Ti_2(PO_4)_3$/C NASICON-type phosphate is introduced as a new anode material for lithium-ion batteries (LIBs). $Ni_{0.5}Ti_2(PO_4)_3$/C was synthesized through the sol–gel route and delivered some remarkable electrochemical performances. Specifically, the $Ni_{0.5}Ti_2(PO_4)_3$/C electrode demonstrates a high rate capability performance and delivers high reversible capacities ranging from 130 mAh g^{-1} to about 111 mAh g^{-1} at current rates ranging from 0.1 C to 5 C in the voltage window of 1.85–3 V (vs. Li^+/Li). In the same voltage range, the material reaches an initial capacity of 105 mAh g^{-1} with a capacity retention of about 82% after 1000 cycles at the high current rate of 10 C. The electrodes are also tested in the wider voltage range of 0.5–3 V (vs. Li^+/Li) and show good reversibility and rate capability performance. Moreover, the $Ni_{0.5}Ti_2(PO_4)_3$/C electrodes enable fast Li^+ diffusion (in the order of 10^{-13} cm^2 s^{-1}) compared with other NASICON-type materials. As a result, a first discharge capacity of 480 mAh g^{-1} is reached.

Introduction

Research and development of energy storage materials are considered as high priority topics owing to their key role in the development and use of clean and renewable energy sources as alternatives to fossil fuels.[1,2] Because of their high energy density, energy efficiency, long cycle life, and the continuous drop in their cost, lithium-ion batteries (LIBs) are considered as some of the most promising energy devices for the portable electronics and electric vehicles (EVs) markets.[3–6] However, LIBs still suffer from safety issues related to the formation of metallic lithium (dendrite) when using graphite as an anode material because of the low plateau voltage (≈0.1 V).[7,8] With the aim of finding safer alternatives to be used as anodes for LIBs, many research efforts have been made to investigate new materials providing good and stable electrochemical performance and better safety conditions than graphite.[8,9]

Among the panoply of known materials, phosphate-based materials provide attractive properties such as long cycling life, good structural stability, better safety, and high ionic conductivity, and are thus considered as promising electrode materials for LIBs, as well as sodium-ion batteries (SIBs).[10–12] As part of this compound class, NASICON-type materials with the general formula $A_xMM'(PO_4)_3$ where "A" can be either monovalent (Li^+, Na^+) or divalent (e.g., Mg^{2+}, Ca^{2+}, Mn^{2+}) ions and M and M′ are transition metals (e.g., Ti, Fe, V, Zr, Sc), stand as potential candidates that can be used either as electrode materials or as solid electrolytes for both LIBs and SIBs.[5,11,13]

Among the NASICON materials, the $A_{0.5}Ti_2(PO_4)_3$ family, where A is a divalent ion (e.g., Mn^{2+}, Mg^{2+}, Ca^{2+}, Fe^{2+}), is being considered for negative electrodes for LIBs and SIBs, because of the low working voltage (≈2.5 vs. Li^+/Li and ≈2.2 vs. Na^+/Na), as well as the empty sites that these compounds provide for lithium (or sodium) hosting (3.5 empty sites).[14–17] Nevertheless, $Ni_{0.5}Ti_2(PO_4)_3$ has not been reported to date although Ni^{2+} is the cation exhibiting the ionic radius closest to that of Li^+. This property could be considered as an advantage for the lithium-ion insertion during electrochemical cycling as a result of a better diffusion of Li^+ inside the existing channels, as reported by Wu et al. in their interesting review regarding the use of NASICON-type phosphates as solid electrolytes for all-solid-state lithium batteries.[18] According to these authors, the high Li^+ ionic conductivity can be only achieved as the channel size of the NASICON framework structure is comparable to the ion size.

[a] Dr. M. Srout, Prof. I. Saadoune
LCME, Faculty of Science and Technology
Cadi Ayyad University, Av. A. El Khattabi, P.B. 549 Marrakesh (Morocco)
E-mail: i.saadoune@uca.ma

[b] Dr. M. Srout, Dr. N. H. Kwon, Prof. K. M. Fromm
Department of Chemistry, University of Fribourg
Chemin du Musee 9, 1700 Fribourg (Switzerland)

[c] Prof. I. Saadoune
Mohammed VI Polytechnic University
Lot 660-Hay Moulay Rachid, Ben Guerir (Morocco)

[d] Dr. W. Luo, Prof. A. Züttel
Laboratory of Materials for Renewable Energy (LMER), Institute of Chemical Sciences and Engineering (ISIC), Basic Science Faculty (SB), École Polytechnique Fédérale de Lausanne (EPFL) Valais/Wallis, Energypolis
Rue de l'Industrie 17, 1951 Sion (Switzerland)

[e] Dr. W. Luo, Prof. A. Züttel
Empa Materials Science & Technology
8600 Dübendorf (Switzerland)

Similarly to the known $Li_4Ti_5O_5$ anode material, $A_{0.5}Ti_2(PO_4)_3$ materials offer a minimum chance for the formation of a solid–electrolyte interphase (SEI) and lithium dendrites owing to the relatively higher working voltage corresponding to titanium (Ti) redox reactions (≈1.5 V for $Li_4Ti_5O_{12}$ and ≈2.5 V for $A_{0.5}Ti_2(PO_4)_3$ materials) compared with graphite (≈0.1 V). The electrochemical behavior of the $A_{0.5}Ti_2(PO_4)_3$ materials is based on a two-step lithium insertion/extraction mechanism owing to the existence of two different vacant sites for lithium intercalation, whereas in $Li_4Ti_5O_5$ anodes, with spinel structures, the insertion mechanism is based on a two-phase step, where lithium is inserted into the vacant site (16*c*) and at the same time structural lithium ions existing in the structure migrate from their structural site (8*a*) to the new hosting site (16*c*).[19,20]

Herein, we report the optimization of the synthesis process of a new NASICON-structured electrode material, $Ni_{0.5}Ti_2(PO_4)_3$/C (NTP@C), and its electrochemical behavior as a novel anode material for use in Li-ion batteries within two potential ranges, 1.85–3.0 V and 0.5–3.0 V. Furthermore, an analysis of the structure, morphology, and electrochemical kinetics of the as-prepared NTP@C material are provided.

Results and Discussion

Structure and morphology

NASICON-type $Ni_{0.5}Ti_2(PO_4)_3$ was reported to be a thermodynamically unstable material that decomposes easily to an oxyphosphate phase.[21,22] With the aim of optimizing the synthesis conditions related to this $Ni_{0.5}Ti_2(PO_4)_3$ NASICON material, its crystallization process was followed by X-ray powder diffraction in the temperature range 660–700 °C. As demonstrated in Figure 1 a, at a temperature of 660 °C, only some characteristic peaks related to the TiP_2O_7 phase appear. At 680 °C, the XRD pattern shows the crystallization of the material as a NASICON phase (space group $R\bar{3}$) with minor impurity traces of TiP_2O_7 (≈3 %) and $Ni_{0.5}TiOPO_4$ (≈3 %). At 700 °C, the NASICON structure of the material was preserved but the appearance of more intense TiP_2O_7 and $Ni_{0.5}TiOPO_4$ related peaks compared with the ones obtained at 680 °C was observed.

Based on these results, only the $Ni_{0.5}Ti_2(PO_4)_3$ material obtained at 680 °C was considered for the following characterizations. At this synthesis temperature, the peaks identified as the NASICON crystalline phase were indexed by assuming a rhombohedral symmetry (space group $R\bar{3}$).

In the $R\bar{3}$ space group, the structure of the material (see the Supporting Information, Figure S1) is built from lantern-like units in sequence along the *c*-axis and each unit is composed of four [TiO_6] octahedra and two [PO_4] tetrahedra sharing O atoms as corners.[11] Theoretically, Ni^{2+} ions occupy only the more stable 3*a* site, leaving more vacant voids at the 3*b* sites.[16,17]

Moreover, the carbon content in the NTP@C composite material was qualitatively determined by Raman spectroscopy as XRD analysis was unable to prove the presence of carbon in an amorphous form. Indeed, the Raman spectra of the NTP pristine powder (Figure 1 b) shows the presence of all characteristic modes related to the NASICON-type structure,[23] whereas the spectra related to the NTP@C composite shown in Figure 1 c show two extra broad bands situated at approximately 1353 and 1589 cm^{-1}, corresponding to the D and G bands of carbon, respectively. Furthermore, TGA (Figure 1 d) was used for quantifying the amount of carbon in the NTP@C composite material, which was measured to be approximately 5.7 wt % carbon of the total weight of the composite. BET measurements on both pristine and carbon-coated NTP powders reveal surface areas of 12.43 $m^2 g^{-1}$ and 13.60 $m^2 g^{-1}$, respectively.

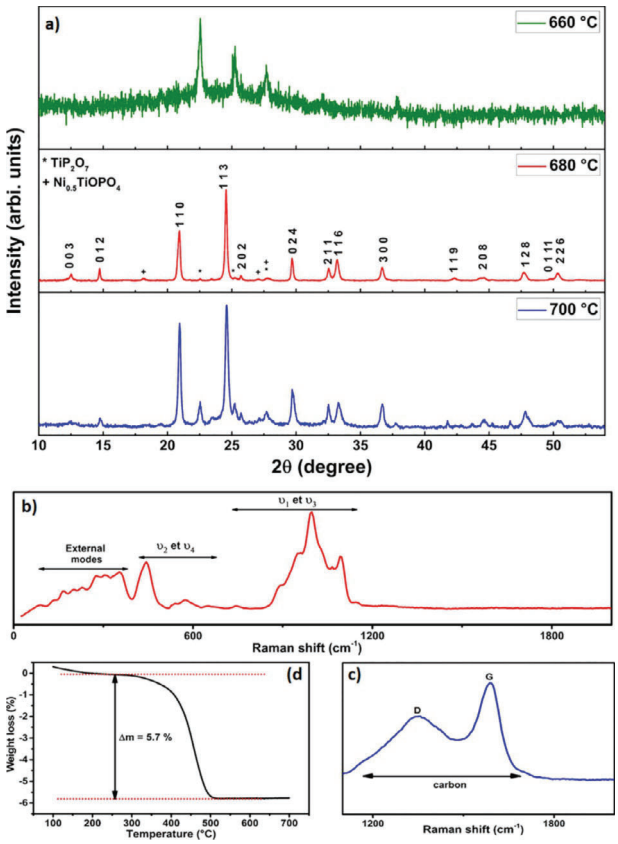

Figure 1. a) XRD patterns of the NTP material at different calcination temperatures. b) Raman spectra of the NTP pristine powder. c) Raman spectra of the NTP@C composite material. d) TGA measurements of NTP@C material.

The morphologies of the NTP and NTP@C materials were examined by SEM and TEM techniques. As shown in the SEM images (Figure 2 a,b), NTP and NTP@C exhibit nano-sized primary particles ranging from approximately 70 to 100 nm with agglomerates. The corresponding TEM images (Figure 2 c,d) confirmed these results and demonstrated that the shape of the primary particles is considered as spherical. Figure 2 d also gives clear insight into how the NTP primary nanoparticles and agglomerates are embedded in the amorphous carbon matrix.

Electrochemical properties

The electrochemical behavior of the NTP@C material was evaluated based on the galvanostatic tests at two different potential windows, 1.85–3 V and 0.5–3 V, and further confirmed by cyclic voltammograms.

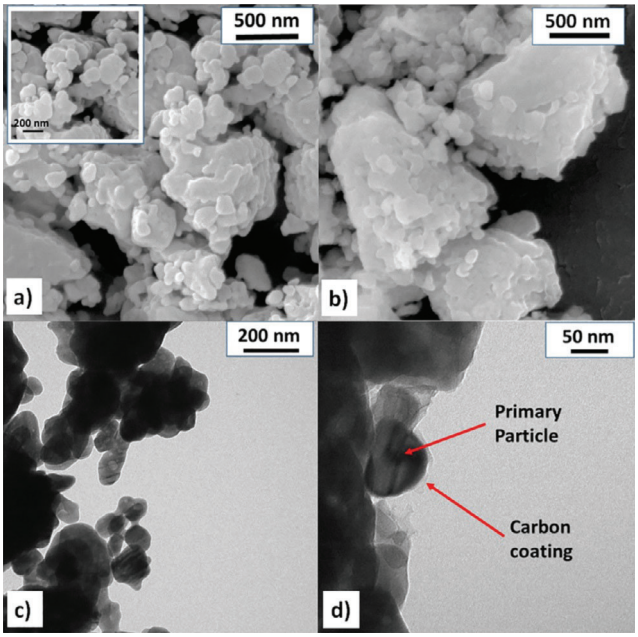

Figure 2. a) SEM image of the NTP material. b) SEM image of the NTP@C composite. c) TEM image of the NTP material. d) TEM image of the NTP@C composite.

Potential window 1.85–3 V

Figure 3a shows the voltage profiles of the NTP@C electrode material versus Li^+/Li in a half-electrochemical cell, during the first five cycles. The lithiation was conducted at 0.1 C current rate in the potential range 1.85–3.0 V (vs. Li^+/Li). In this voltage range, the theoretical capacity of the NTP@C material corresponding to the insertion of two Li^+ into the structure is about 130 mAh g^{-1}. This theoretical capacity is calculated by considering the reduction of two Ti^{4+} to Ti^{3+}, normally taking place at the voltage approaching 2.48 V. The experimental capacity recorded at the potential plateau of 2.48 V is equal to 123 mAh g^{-1}, which is close to the theoretical one. Note that, the overall experimental capacity (considering the voltage cut-off of 1.85 V) delivered at the first discharge is about 200 mAh g^{-1}, which drops to approximately 136 mAh g^{-1} during the four subsequent cycles. The small capacity excess is probably due to the contribution of the electrochemically active impurity phase. Furthermore, the obtained extra capacity during the first discharge can also be attributed to the formation of an SEI layer even though we are above 1 V.

The voltage difference between the first discharge profile and the following ones can be attributed to the active material environment changes that take place after the first Li^+ insertion into the structure at the first discharge.

Figure 3a, inset, shows the first five CV curves of the NTP@C material (vs. Li/Li^+). During the first discharge, one large peak is observed, reaching its highest intensity at about 2.04 V related to the reduction of Ti^{4+} to Ti^{3+}.[24] After the first cycle, two peaks are observed during charging at 2.53 V and 2.8 V, then at 2.78 V and 2.44 V during discharge. These peaks are due to lithium (dis)insertion (out of) into the NTP@C structure, while reducing and oxidizing titanium (Ti^{4+}/Ti^{3+}), confirming the obtained galvanostatic results. The observation of these separated peaks is attributed to lithium insertion into two thermodynamically different vacant sites (M1 and M2).[14,16]

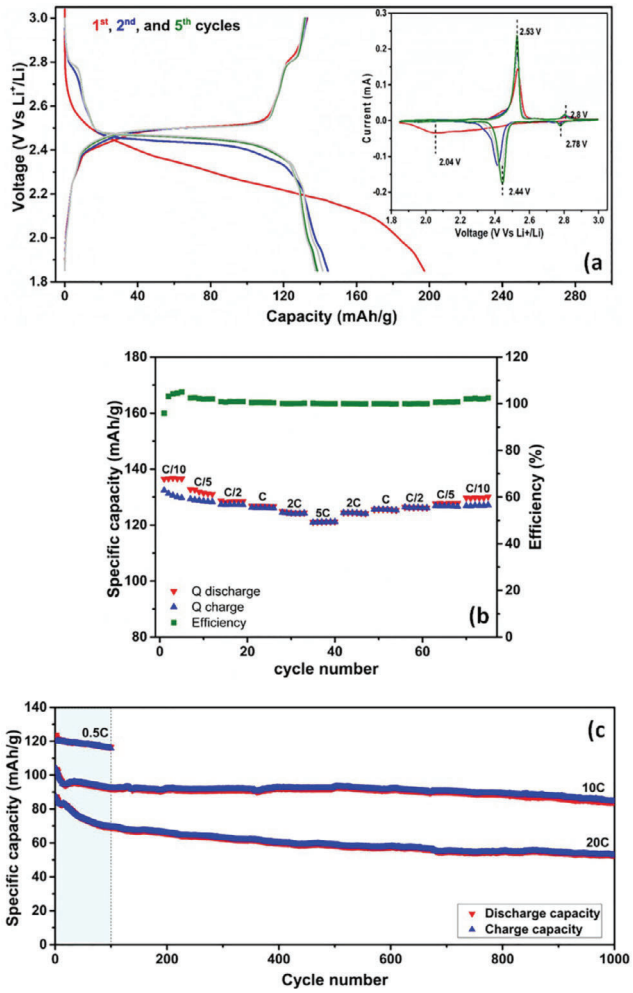

Figure 3. Electrochemical properties of the NTP@C electrode material in the potential range 1.85 V–3 V. a) Charge/discharge curves at 0.1 C—corresponding cyclic voltammetry at a scan rate of 0.02 mV s^{-1}. b) Rate capability and c) long-term cycling performance at different current rates 0.5 C (100 cycles), 10 C (1000 cycles), and 20 C (1000 cycles).

For comparison, the electrochemical behavior and rate performance of the NTP material (without carbon coating) were also tested. The NTP material showed a lower electrochemical rate performance than the NTP@C (Figure S2b), whereas the galvanostatic cycling profiles were analogous (Figure S2a), confirming the importance of the carbon coating in the phosphate-based materials, to improve their electronic conductivity and consequently improve their electrochemical performance. Accordingly, EIS measurements of both NTP and NTP@C electrode materials were obtained. The Nyquist plots of both materials at the open circuit voltage (OCV) showed quite similar profiles (Figure S3a), whereas after 20 cycles at the current rate of 1 C, within the voltage range 1.85–3.0 V, the Nyquist plots were different (Figure S3b). When the obtained curves were fitted, R values related to the electrolyte resistance (R_s), the solid electrolyte interphase (SEI) layer resistance (R_{SEI}), the elec-

tronic conductivity of the active material (R_e), and the charge-transfer resistance (R_{ct}) of the NTP@C composite were smaller than those obtained for the non-coated NTP material (Table S2), confirming the effectiveness of the applied carbon coating to improve the electrochemical kinetics of the studied composite.

Furthermore, compared with other titanium-based NASICON materials used as anodes for lithium-ion batteries,[23,25–27] NTP@C delivered superior rate capability performances (Figure 3b). Capacities of about 130 mAh g^{-1} and more than 110 mAh g^{-1} were attained at current rates of 0.1 C and 5 C, respectively. This superior performance can be linked to the presence of nickel (Ni) in the structure. The ionic radius of Ni is of the same order as that of lithium, which provides an optimized channel size for lithium ion intercalation, and therefore better Li^+ ionic conductivity.[18] Moreover, Ni provides better electronic conductivity compared with that provided by Li or Mg.

Inspired by the relatively superior rate performance of the NTP@C material, the long-term cycling stability was also investigated at different current rates of 0.5 C, 10 C, and 20 C (Figure 3c), where the first three cycles were measured at a current rate of 0.1 C in all three measurements.

The NTP@C electrode material delivered a capacity retention of about 96% after 100 cycles at the current rate of 0.5 C. The capacity retention decreases slightly after cycling the material at a much higher current rate of 10 C. After 1000 cycles, the capacity retention is around 82%. At the very high current rate of 20 C, the capacity fades clearly during the first 200 cycles before it is stabilized, and only a capacity retention of about 62% was obtained. These remarkable rate performances confirm the structural (mechanical) stability of the studied electrode upon cycling. To support this, we recovered the electrode material after 100 cycles under a current rate of 20 C, within the potential window of 1.85–3 V. The recovered sample (at 3 V) was analyzed by SEM and its morphology was compared with the pristine material. No clear change in the morphology nor in the particle size of the cycled phosphate was detected (Figure S5). The open 3D framework of the NASICON structure, offering a large available crystallographic site for lithium insertion, leads in fact to low volume variation of the electrode material, avoiding any mechanical degradation upon repeated Li insertion/extraction.

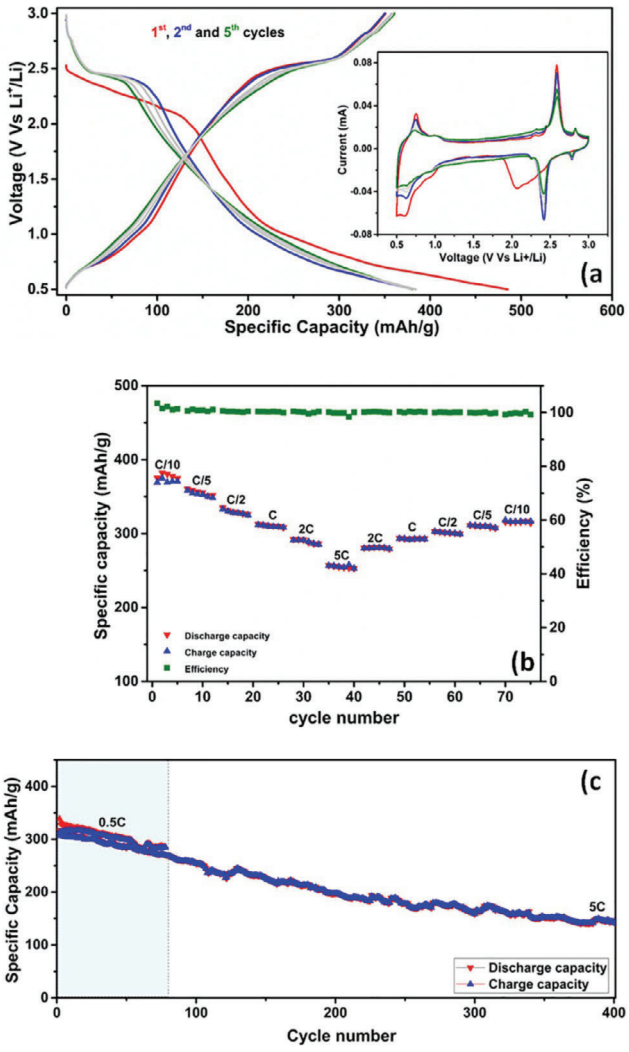

Figure 4. Electrochemical properties of the NTP@C electrode material in the potential range 0.5 V–3 V. a) Charge/discharge curves at 0.1 C—corresponding cyclic voltammetry at a scan rate of 0.02 mV s^{-1}. b) Rate capability and c) long-term cycling performance at different current rates 0.5 C (80 cycles), 5 C (400 cycles).

Potential window 0.5 V–3 V

As shown in Figure 4a, unlike some other NASICON structure-type materials,[28] the NTP@C material showed a first charge/discharge profile that is very similar to the four subsequent ones upon cycling between 0.5 and 3 V, revealing a good structural stability at this voltage range. This result was also confirmed by cyclic voltammetry. This better structural stability can be directly related to the presence of Ni, which contributes to the formation of a structural network with stronger "covalent" bonds with oxygen (O) than for Li in the $LiTi_2(PO_4)_3$ material. Also, providing an extra 0.5 empty void for Li insertion when using divalent ions such as Ni^{2+} instead of Li^+ can also lead to better structural stability.

At this potential range, the material delivered a first discharge capacity of about 480 mAh g^{-1} at a current rate of 0.1 C. This capacity dropped to about 380 mAh g^{-1} after the first cycle and stabilized at the same value for the four subsequent cycles. During the first discharge, a first plateau was observed between 2.5 and 2.1 V, which is attributed to the reduction of Ti^{4+} to Ti^{3+} following the reaction mechanism:

$$Ni_{0.5}Ti_2^{IV}(PO_4)_3 + 2\,Li^+ + 2\,e^- \leftrightarrow Li_2Ni_{0.5}Ti_2^{III}(PO_4)_3$$

Another plateau was observed around 0.7–0.6 V (about 1.7 V lower than the first plateau), which can be attributed to the reduction of Ti^{3+} to Ti^{2+} and also the formation of an SEI layer.[16]

$$Li_2Ni_{0.5}Ti_2^{III}(PO_4)_3 + 2\,Li^+ + 2\,e^- \leftrightarrow Li_4Ni_{0.5}Ti_2^{II}(PO_4)_3$$

These obtained plateaus were in very good agreement with the different cyclic voltammetry obtained peaks (inset of Figure 4a).

The structural stability of the NTP@C material during the first galvanostatic cycle at this widened voltage range (0.5–3.0 V) was also investigated. Ex situ XRD measurements at different states of discharge and charge confirmed that all characteristic peaks related to the NASICON structure were preserved while inserting/extracting lithium into/out of the structure, although the diffraction peaks became broader as a result of the decrease in the phosphate crystallinity (Figure S4). This good reversibility of the NTP@C material during the first galvanostatic cycle at this wide voltage range was also confirmed with XPS by following changes in the valence state and the atomic ratio of Ti and Ni after the first cycle. As a reference, XPS measurement of the NTP@C electrode at the OCV was executed. For the as-prepared electrodes, no Ni or Ti could be detected by XPS, although other elements such as C, F, and O were easily detectable, indicating the presence of the SEI and electrolyte residues on the electrode surface (Figure S7). An SEM image of the electrode discharged to 0.5 V (Figure S5) confirmed the presence of a thick homogeneous layer of SEI on the electrode surface explaining the limited signal (no Ti, Ni signals) detected by XPS (analysis depth max 10 nm). However, after sputtering the electrode with Ar^+ ions (etching), peaks of Ni and Ti were detected (Figure S8). At the OCV, the Ti $2p_{3/2}$ peak of the NTP@C electrode was observed at approximately 459 eV, which is consistent with that of Ti^{4+}.[29] After the first cycle, the oxidation state of Ti was recovered to the initial oxidation state obtained at the OCV. Even though Ar^+ sputtering could slightly reduce the Ti^{4+} to Ti^{3+},[30] shown as a small shoulder in the Ti 2p spectrum, the similar Ti^{4+}/Ti^{3+} ratios of the two samples can be an indicator of their comparable oxidation states. The similar Ti/Ni atomic ratio ($\approx$5.0), calculated by normalizing the Ti $2p_{3/2}$ and Ni $2p_{3/2}$ peak area to their atomic selectivity factors[31] of the two samples also indicates that the surface composition does not change after one charge/discharge cycle. Further, SEM images of pristine and cycled electrodes showed no significant changes in the morphology of the active material after one cycle (Figure S5).

Moreover, to further study the electrochemical performance stability of the NTP@C electrode material, long-term galvanostatic cycling measurements were performed at current rates of 0.5 C (80 cycles) and 5 C (400 cycles). As shown in Figure 4c, a significant capacity fading was observed for both measurements. This capacity fading can be directly related to the structural changes that take place after the first few cycles. Once the NTP@C electrode material is discharged to 0.5 V, at least four Li^+ are inserted into the structure, which is more than the NASICON structure of the NTP@C material can theoretically host (3.5 vacant sites).

Ex situ XRD patterns of the NTP@C electrodes after cycling (Figure S6), show that the NASICON structure of the NTP material can resist the massive Li^+ insertion during the first cycle (more than 3.5 Li^+), but after 80 cycles at a current rate of 0.5 C, and 500 cycles at the current rate of 5 C, all the NASICON structure characteristic peaks disappeared, confirming the structural changes of the NTP@C material, and consequently leading to the observed capacity fading.

The rate capability of the NTP@C material was also tested in this potential range. Even with the noticed structural changes that take place during the long-term cycling measurements, the material showed a relatively good reversibility and high coulombic efficiency at different current rates ranging from 0.1 C to 5 C. The NTP@C electrode material delivered its highest capacity of about 370 mAh g^{-1} at a slow current rate of 0.1 C, whereas the lowest one was obtained at the high current rate of 5 C with an average value of about 250 mAh g^{-1}. When switching back to a 0.1 C rate, the electrode material recovered a capacity of around 315 mAh g^{-1} (Figure 4b).

Electrochemical kinetics of lithium ions

To better understand the lithium diffusion kinetics leading to the good electrochemical performances of the NTP@C material, the galvanostatic intermittent titration technique (GITT) and cyclic voltammetry (CV) were used to calculate the electrochemical lithium diffusion coefficient D_{Li^+} during the first lithiation process. Figure 5a shows the GITT curve during the first discharge at the rate of 0.05 C (insertion of 0.1 Li^+ into the structure for 2 h, then relaxation for 16 h to reach the thermodynamic equilibrium). This measurement demonstrates a slight polarization at both plateaus related to the reduction of Ti cations (Ti^{4+}/Ti^{3+} around 2.4 V and Ti^{3+}/Ti^{2+} at 0.6 V) during the lithiation process, whereas more important polarization is noticed far from the mentioned plateaus. Moreover, the inset of Figure 5a shows a single GITT step at around 2.36 V. The cell voltage during titration is considered to be linearly proportional to $\tau^{1/2}$ (Figure S9). Then, based on Fick's second law of diffusion, the diffusion coefficient of lithium in the NTP@C material can be calculated by considering the following simplified Equation (1):[32–34]

$$D_{Li^+} = \frac{4}{\pi\tau}\left(\frac{n_B V_m}{S}\right)^2\left(\frac{\Delta E_s}{\Delta E_\tau}\right)^2 \quad (1)$$

where τ is the duration of the current pulse (s), n_B is the number of moles (mol), V_m is the molar volume of the active materials in the electrode ($cm^3\,mol^{-1}$), S is the electrode/electrolyte contact area (cm^2), ΔE_s is the change of the steady-state (equilibrium) voltage owing to the current pulse, and ΔE_τ is the total change in the cell voltage during the constant current pulse, neglecting the *IR* drop. τ, ΔE_s, and ΔE_τ are labeled in the inset of Figure 5a.

Figure 5b shows the variation of the calculated D_{Li^+} as a function of the voltage during the discharge process. The calculated values of D_{Li^+} ranged between 1.21×10^{-12} and $1.2\times10^{-15}\,cm^2\,s^{-1}$, with an average of approximately $1.08\times10^{-13}\,cm^2\,s^{-1}$. D_{Li^+} fluctuations towards a lower diffusion coefficient are observed around the same voltage as the reduction peaks in the CV curve. This might be attributed to the different changes (structural, electronics) that take place while inserting Li^+ into the structure.

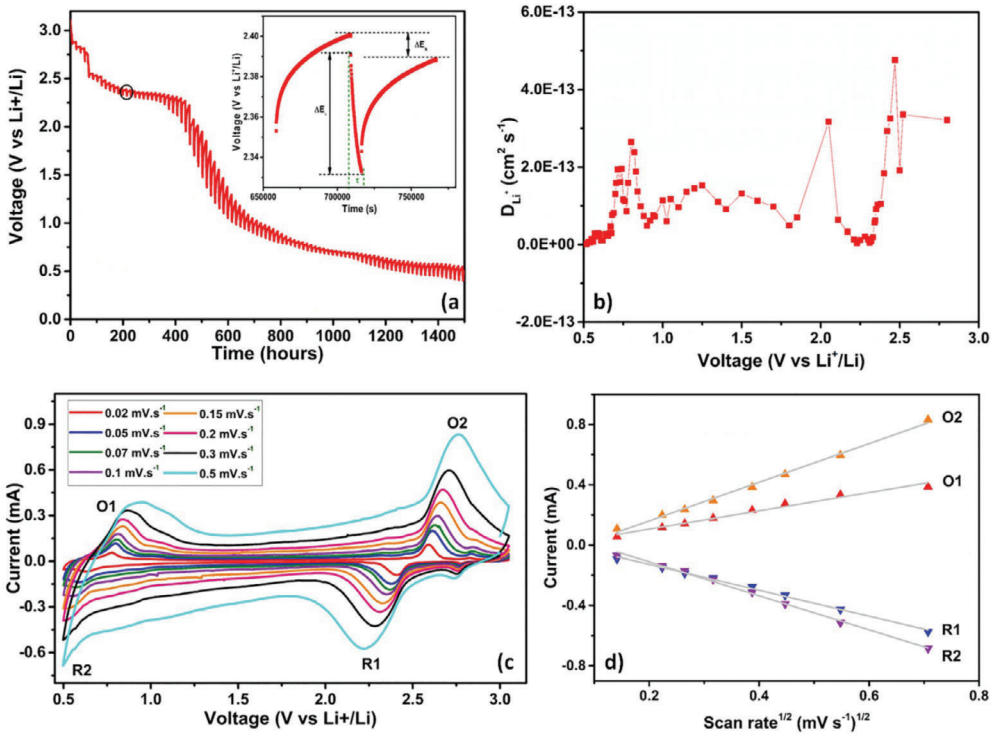

Figure 5. Electrochemical kinetics of the NTP@C material in the range 0.5–3.0 V. a) GITT curve during the first discharge (inset: one GITT step around 2.38 V). b) Lithium diffusion coefficient during the first discharge. c) CV at different scan rates. d) Linear relationship between the current peaks and the square root of the scan rates.

The cyclic voltammetry technique was also used to determine the kinetics of Li^+ insertion and extraction in the NTP@C electrode. The major reversible cathodic reduction and anodic oxidation of $Ti^{4+/3+}$ occurred at 2.36 and 2.64 V (vs. Li^+/Li), respectively, by using a scan rate of 0.1 mV s^{-1}, which correspond to the insertion and extraction processes of Li^+, respectively (Figure 5c). Another redox reaction is observed at a potential of 0.7 V (vs. Li^+/Li), but the current intensity is lower than that at higher potential. The potential difference between anodic and cathodic peaks becomes narrower with decreasing scan rate.

Figure 5d shows that the cathodic and the anodic current peaks are linearly dependent on the square root of the scan rate (R^2 of 0.9963, 0.9962, 0.9813, and 0.9957 for cathodic and anodic lines, respectively). Based on this relationship, the Li^+ diffusion coefficient D_{Li^+} in the NTP@C electrode was calculated by using the Randles–Sevcik equation [Eq. (2)]:[35]

$$I_p = (2.69 \times 10^5)\, n^{3/2}\, S\, D_{Li^+}{}^{1/2}\, C\, \upsilon^{1/2} \qquad (2)$$

where I_p is the current peak (mA), n is the number of electrons, S is the surface area of the electrode (cm^2 g^{-1}), D is the diffusion coefficient (cm^2 s^{-1}), C is the concentration of Li^+ (mol cm^{-3}), and υ is the scan rate (mV s^{-1}).

The calculated D_{Li^+} for the insertion of Li^+ in the NTP@C was 3.42×10^{-13} cm^2 s^{-1}, whereas that for the extraction of Li^+ was 7.38×10^{-13} cm^2 s^{-1} at 25 °C. D_{Li^+} at 0.7 V (vs. Li^+/Li) and scan rates between 0.02 and 0.1 mV s^{-1} was 3.89×10^{-13} and 2.22×10^{-13} cm^2 s^{-1} for the insertion and extraction of Li^+, respectively, which are similar to the ones at higher potential (2.7 V). Overall, these values are of the same order as the average value obtained by the GITT method. They are higher than the D_{Li^+} of $LiTi_2(PO_4)_3$ (1.31×10^{-14} and 1.55×10^{-14} cm^2 s^{-1} for the insertion and the extraction of Li^+, respectively) by using the same technique.[36]

When the lower cut-off voltage of the CV measurement was increased to 1.85 V instead of 0.5 V (vs. Li^+/Li), the current densities were increased (Figure S10a). D_{Li^+} was 2.54×10^{-12} and 8.0×10^{-13} cm^2 s^{-1} for the anodic oxidation and cathodic reduction, respectively. Specifically, the diffusion coefficient of the extraction of Li^+ is one order of magnitude higher than that of the extended voltage window between 0.5 and 3 V (vs. Li^+/Li). This higher diffusion coefficient can be directly related to the structural stability of NTP@C in this voltage range. In addition, the voltage difference between the anodic and the cathodic potential is 0.4 V for the range between 1.85 and 3 V (vs. Li^+/Li), whereas it is 0.7 V in the range 0.5–3 V (vs. Li^+/Li) at the scan rate of 0.5 mV s^{-1}. This indicates that the lower cut-off potential increases the resistance of lithium ion diffusion.

Conclusions

NTP NASICON material was synthesized by the sol–gel route and carbon-coated by using sucrose as the carbon source to obtain the NTP@C composite material. The physicochemical and electrochemical properties of both materials were investigated. When tested as anode material for Li-ion batteries, NTP@C showed a high reversible capacity, an excellent rate ca-

pability, and very stable long-term cycling performance at the voltage range of 1.85–3.0 V (vs. Li^+/Li). At a wider voltage window of 0.5–3.0 V, the NTP@C electrode material also showed a good reversibility and good rate capability but capacity fading was noted during the long-term cycling tests. This capacity fading was related to the structural changes that take place after some cycles in this voltage window. Based on more the detailed study of Li^+ diffusion kinetics in the NTP@C by using GITT and CV techniques, the improved electrochemical performance of this material results from its high Li^+ diffusion coefficient compared with the one calculated for $LiTi_2(PO_4)_3$.

Experimental Section

Synthesis and characterization

The synthesis of the $Ni_{0.5}Ti_2(PO_4)_3$ (NTP) NASICON-type material was accomplished by the conventional sol–gel synthesis route, by mixing stoichiometric amounts of $C_4H_6NiO_4{\cdot}4H_2O$ (99.0%; Sigma–Aldrich) dissolved in ethanol, H_3PO_4 (85.8%; Sigma–Aldrich), and $TiCl_4$ solution (99.0%; Sigma–Aldrich) diluted in ethanol. After mixing for about 2 h, a gel was obtained. The gel was then dried at 90 °C for 24 h and calcined at 680 °C for 12 h under air. This synthesis temperature was selected as the best after numerous attempts in a narrow temperature range (660–700 °C). The resulting NTP powder (85 wt%) was ground with 15 wt% sucrose in acetone, then the mixture was dried and annealed at 600 °C for 5 h under an argon flow. The final $Ni_{0.5}Ti_2(PO_4)_3$/C (NTP@C) composite material was black. The phase structure and morphology of the prepared NTP and NTP@C material were characterized by powder X-ray diffraction (XRD, Rigaku Ultima IV, CuK_α radiation), Raman spectroscopy (Cofotec MR520 3D Raman confocal microscope; 532 nm beam), field-emission scanning electron microscopy (SEM, TESCAN Mira 3 LM field emission), and field-emission transmission electron microscopy (TEM, FEI Tecnai Spirit). The specific surface area of the NTP and NTP@C materials was determined at 77 K by using the Brunauer–Emmett–Teller (BET) method with a Gemini VII 2390 Surface Area Analyzer (Micromeritics Instrument Corp.). The degassing conditions were set to be 200 °C for 24 h for both samples. The carbon content in the composite material was determined by thermogravimetric analysis (TGA), with a heating rate of 10 °C min^{-1} by using a Discovery TGA instrument under air atmosphere. The X-ray photoelectron spectroscopy (XPS) data were collected with a SPECS Phoibos 100 spectrometer using MgK_α X-ray. Samples were transferred into the XPS chamber through a glovebox without exposure to air. To remove the electrolyte residues on the surface, samples were sputtered using Ar^+ prior to the XPS measurement. The binding energy was corrected by using the C 1s peak at 285 eV.

Electrochemical measurements

Electrodes were prepared by blending 75 wt% NTP@C active materials, 15 wt% Super P as the conductive additive, and 10 wt% carboxymethyl cellulose (CMC) as a binder dissolved in distilled water. The obtained slurry was then pasted onto a cooper foil and dried at 80 °C for 12 h in a vacuum chamber. The electrodes were cut into discs with two different diameters, 11 and 12.6 mm with an active material mass load of around 1–2 mg cm^{-2}. Metallic lithium foil was used as the counter and reference electrodes. Commercial Celgard was used as a separator. The used electrolyte was 1 M $LiPF_6$ dissolved in ethylene carbonate (EC) and dimethylcarbonate (DMC, 50:50), 1 M. Electrochemical tests were performed with CR2032 coin cells. Cells were assembled in an argon-filled glovebox with water and oxygen contents below 0.1 ppm. The cells were electrochemically tested at two different potential ranges of 1.85–3.0 V and 0.5–3.0 V vs. Li^+/Li. The electrochemical tests were carried out with MPGE (Biologic instrument), Arbin instrument, and Autolab (Metrohm autolab) instruments. Electrochemical impedance spectroscopy (EIS) tests were performed by using an SP150 Biologic instrument.

Acknowledgements

This work was done with the financial support of the OCP group (Morocco) through the APPHOS Program (2017–2019). The authors further thank the Swiss Confederation for the excellence stipend for M. Srout, the University of Fribourg and the Swiss National Science Foundation, as well as the Adolphe Merkle Foundation for generous support. Many thanks go to Prof. Bouchaib Manoun for scientific discussions.

Conflict of interest

The authors declare no conflict of interest.

Keywords: batteries · electrodes · lithium · NASICON · phosphates

[1] G. G. Eshetu, T. Diemant, M. Hekmatfar, S. Grugeon, R. J. Behm, S. Laruelle, M. Armand, S. Passerini, *Nano Energy* **2019**, *55*, 327–340.
[2] J. B. Goodenough, *Nat. Electron.* **2018**, *1*, 204.
[3] B. Scrosati, J. Garche, *J. Power Sources* **2010**, *195*, 2419–2430.
[4] J. W. Choi, D. Aurbach, *Nat. Rev. Mater.* **2016**, *1*, 16013.
[5] F. Zheng, M. Kotobuki, S. Song, M. O. Lai, L. Lu, *J. Power Sources* **2018**, *389*, 198–213.
[6] L. Ji, Z. Lin, M. Alcoutlabi, X. Zhang, *Energy Environ. Sci.* **2011**, *4*, 2682–2689.
[7] Y. Lu, L. Yu, X. W. D. Lou, *Chem* **2018**, *4*, 972–996.
[8] G. N. Zhu, Y. G. Wang, Y. Y. Xia, *Energy Environ. Sci.* **2012**, *5*, 6652–6667.
[9] P. Roy, S. K. Srivastava, *J. Mater. Chem. A* **2015**, *3*, 2454–2484.
[10] C. Masquelier, L. Croguennec, *Chem. Rev.* **2013**, *113*, 6552–6591.
[11] Z. Jian, Y.-S. Hu, X. Ji, W. Chen, *Adv. Mater.* **2017**, *29*, 1601925.
[12] S. Chen, C. Wu, L. Shen, C. Zhu, Y. Huang, K. Xi, J. Maier, Y. Yu, *Adv. Mater.* **2017**, *29*, 1–21.
[13] S. Difi, A. Nassiri, I. Saadoune, M. Sougrati, P. Lippens, *J. Phys. Chem. C* **2018**, *122*, 11194–11203.
[14] A. Aatiq, M. Ménétrier, E. Eljazoul, C. Delmas, *Solid State Ionics* **2002**, *150*, 391–405.
[15] R. Essehli, B. El Bali, A. Faik, M. Naji, S. Benmokhtar, Y. R. Zhong, L. W. Su, Z. Zhou, J. Kim, K. Kang, M. Dusek, *J. Alloys Compd.* **2014**, *585*, 434–441.
[16] Y. Zhao, Z. Wei, Q. Pang, Y. Wei, Y. Cai, Q. Fu, F. Du, A. Sarapulova, H. Ehrenberg, B. Liu, G. Chen, *ACS Appl. Mater. Interfaces* **2017**, *9*, 4709–4718.
[17] Z. Wei, X. Meng, Y. Yao, Q. Liu, C. Wang, Y. Wei, F. Du, G. Chen, *ACS Appl. Mater. Interfaces* **2016**, *8*, 35336–35341.
[18] Z. Wu, Z. Xie, A. Yoshida, Z. Wang, X. Hao, A. Abudula, G. Guan, *Renewable Sustainable Energy Rev.* **2019**, *109*, 367–385.
[19] A. Mahmoud, J. M. Amarilla, I. Saadoune, *Electrochim. Acta* **2015**, *163*, 213–222.
[20] B. Zhao, R. Ran, M. Liu, Z. Shao, *Mater. Sci. Eng. R* **2015**, *98*, 1–71.
[21] P. Gravereau, J. P. Chaminade, B. Manoun, S. Krimi, A. El Jazouli, *Powder Diffr.* **1999**, *14*, 10–15.

[22] I. Belharouak, K. Amine, *Electrochem. Commun.* **2005**, *7*, 648 – 651.
[23] M. Srout, K. Lasri, M. Dahbi, A. Kara, L. Tetard, I. Saadoune, *J. Power Sources* **2019**, *435*, 226803.
[24] A. Aatiq, C. Delmas, A. El Jazouli, *J. Solid State Chem.* **2001**, *158*, 169 – 174.
[25] V. Aravindan, W. C. Ling, S. Hartung, N. Bucher, S. Madhavi, *Chem. Asian J.* **2014**, *9*, 878 – 882.
[26] P. Lavela, G. Ortiz, J. L. Tirado, *Electrochim. Acta* **2012**, *77*, 150 – 156.
[27] S. Yu, H. Tempel, R. Schierholz, Ö. Aslanbas, X. Gao, J. Mertens, L. G. J. de Haart, H. Kungl, R. A. Eichel, *ChemElectroChem* **2016**, *3*, 1157 – 1169.
[28] S. Benmokhtar, A. El Jazouli, S. Krimi, J. P. Chaminade, P. Gravereau, M. Menetrier, D. De Waal, *Mater. Res. Bull.* **2007**, *42*, 892 – 903.
[29] V. V. Atuchin, V. G. Kesler, N. V. Pervukhina, Z. Zhang, *J. Electron Spectrosc. Relat. Phenom.* **2006**, *152*, 18 – 24.
[30] P. Karmakar, G. F. Liu, J. A. Yarmoff, *Phys. Rev. B* **2007**, *76*, 193410.
[31] M. P. Seah, *Surf. Interface Anal.* **1980**, *2*, 222 – 239.
[32] E. Deiss, *Electrochim. Acta* **2005**, *50*, 2927 – 2932.
[33] W. Weppner, *J. Electrochem. Soc.* **1977**, *124*, 1569 – 1578.
[34] Y.-S. Lee, K.-S. Ryu, *Sci. Rep.* **2017**, *7*, 16617.
[35] A. J. Bard, L. R. Faulkner, *Electrochemical Methods Fundamentals and Applications*, 2nd ed., Wiley, Hoboken, **2001**.
[36] H. K. Roh, H. K. Kim, K. C. Roh, K. B. Kim, *RSC Adv.* **2014**, *4*, 31672 – 31677.